Damage Assessment in Composite Material Using Air-Coupled Transducers

Damian Mindykowski(✉), Tomasz Wandowski, Pawel Kudela, Piotr Fiborek, and Maciej Radzienski

Institute of Fluid-Flow Machinery, Polish Academy of Sciences, Fiszera 14 Street, 80–231 Gdansk, Poland
dmindykowski@imp.gda.pl

Abstract. In this paper results of damage assessment of composite panel using guided wave propagation phenomenon are presented. Elastic waves excitation is based on piezoelectric transducer (PZT) and air-coupled transducer (ACT) while the waves sensing is based on scanning laser Doppler vibrometry. It thus forms the full non-contact diagnostic approach. Thin panel made of fibre-reinforced polymer is investigated. The problem of optimal slope angle of ACT and the possibility of symmetric and antisymmetric elastic wave modes excitation is investigated. Contact (PZT) and non-contact (ACT) elastic waves generation methods and their influence on the artificial damage (Teflon inserts) localization results are compared. Moreover, the influence of single and multiple acoustic wave sources on artificial damage localization results and the problem of panel coverage area by elastic waves with large amplitudes to improve damage sensitivity are investigated. Different locations of ACTs and their influence on damage detection results are investigated. Two damage imaging algorithms based on elastic waves root mean square (RMS) energy maps and wavefield irregularity mapping (WIM) have been proposed.

Keywords: Guided waves · Air-Coupled Transducer · Scanning laser Doppler vibrometry · Composite panel

1 Introduction

Nowadays, fibre-reinforced composites are more and more popular in many industrial branches. Safe exploitation of composite structures can be achieved with the utilization of non-destructive testing (NDT) or structural health monitoring (SHM) [1]. Focusing the attention on NDT methods, most popular techniques are related to conventional ultrasonic testing (UT) where hand-held devices are utilized.

Recently, more and more attention is focused on elastic guided waves propagation phenomenon utilization in NDT. Elastic waves propagating in thin plates and panels are called Lamb waves. The main advantage of Lamb waves utilization is small waves energy losses during the long distance propagation. An interesting way to excite Lamb waves in structural elements via non-contact methods is the usage of air-coupled

P. Rizzo and A. Milazzo (Eds.): EWSHM 2022, LNCE 270, pp. 13–23, 2023.
https://doi.org/10.1007/978-3-031-07322-9_2

transducer (ACT) [2]. Elastic waves can be registered using scanning laser Doppler vibrometer (SLDV) [3] or by another ACT [2]. There are different applications of ACT-based techniques for material characterization and structural interrogations. The ACT-based measurement techniques were used for: determination of velocity and attenuation of the ultrasounds in the material [4], measurements of the plate thickness [4], detection of artificial cracks in solar cells [5], detection of delamination in wood and glued timber laminates [6, 7], debonding in aluminium-epoxy-aluminium single lap joints [8] and condition assessment of concrete rail ties [9]. In the research ACT working at frequencies of MHz [2], hundreds of kHz [7] and relatively low frequency - 40 kHz [10, 11] are used. In this paper authors present results of low-frequency ACT (40 kHz) usage for the artificial damage detection and localization in glass fibre-reinforced polymer (GFRP). Such low-frequency ACTs are very popular and cheap transducers that allow achieving good damage localization results in the form of damage maps based on elastic waves energy (RMS) and wavenumber irregularities mapping (WIM).

2 Experimental Set-Up

The experimental setup consisted of scanning laser Doppler vibrometer (SLDV) Polytec PSV-400, arbitrary signal generator, signal amplifier, PC, composite specimen, piezoelectric transducer (PZT) and air-coupled acoustic transducer (ACT). The specimen used in the research was a GFRP panel with dimensions of $500 \times 500 \times \sim 2$ mm. The specimen consisted of twelve layers of VV192T/202 prepregs in the form of fabric with orientations: $[0/90/0/90/0/90]_S$. The specimen contained Teflon inserts with different shapes (T1-T4), what is depicted in the Fig. 1. They are located at the same depth - 0.5 mm from the surface where the laser vibrometry measurements are performed. The usage of Teflon inserts aims to simulate delaminations in the specimens. Elastic waves are excited using the contact method based on piezoelectric transducer and the non-contact method based on ACT. In the case of a PZT, the element in the form of a disc with diameter of 10 mm and thickness of ~ 0.5 mm made out of NCE51 piezoelectric material was utilized. The transducer was bonded in the middle of the specimen using the cyanoacrylate bond agent and it was removed before measurements related to the ACT-based waves generation. ACT with a diameter of 16 mm, length of 12 mm and base excitation frequency of 40 kHz was used. Full wavefield measurements of elastic waves propagation were conducted in on-contact way based on SLDV. The measurements were taken at the surface opposite to the surface where elastic waves were excited by ACT or PZT. Only one scanning head of SLDV was used – the measurements were taken along the laser beam. The measurements were taken at the grid of 375×375 measurement points (points spacing ~ 1.3 mm).

3 Non-contact ACT-Based Elastic Waves Generation

The general idea of non-contact ACT-based elastic waves generation in solids is schematically presented in the Fig. 2. Acoustic waves (sound pressure waves) are generated in the air by ACT. These waves propagate in the air and then, due to interaction of the acoustic waves with the solid, part of the acoustic wave energy is transferred to the solid in the form of elastic waves and part of the acoustic wave energy is related to acoustic waves reflected from the solid. Elastic waves generated in the specimen have the form of shear and axial waves. In the case of plate-like structures as consequence of subsequent internal reflection of shear and axial waves in structure, elastic guided (Lamb) waves. Lamb waves propagate as symmetric and antisymmetric modes. Schematic illustration of the mentioned phenomena is shown Fig. 2.

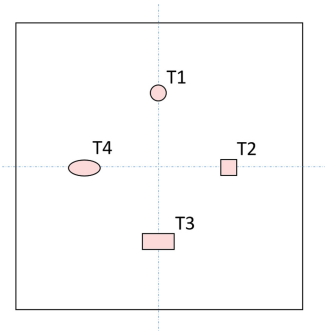

Fig. 1. Investigated specimen (T1-T4 - Teflon inserts).

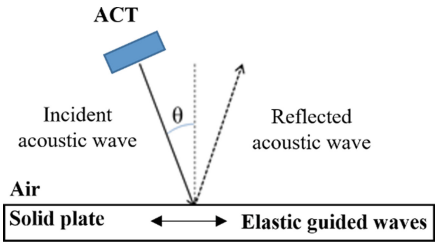

Fig. 2. Schematic illustration of the ACT-based elastic waves generation.

In the Fig. 3 the results of numerical simulation of non-contact elastic waves generation in the specimen using ACT are presented. The simulation was performed in COMSOL software. In Fig. 3a) acoustic waves generated by ACT and propagating in the air are visible. In Fig. 3b) the elastic waves interact with the plate and part of the acoustic waves energy is transformed into elastic waves propagating in the plate.

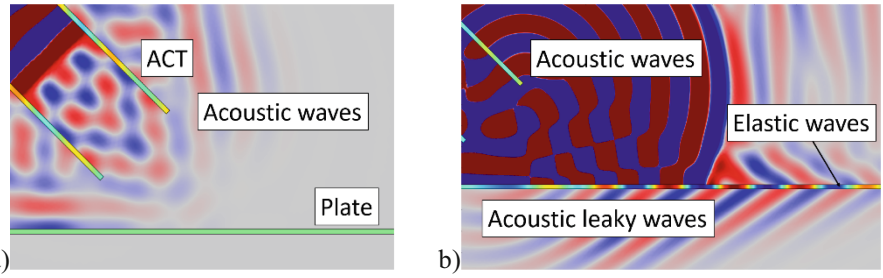

Fig. 3. Results from numerical simulations of the non-contact elastic waves generation: a) generation of the acoustic waves by ACT, b) conversion of the acoustic to elastic waves at the plate surface.

Part of the acoustic waves energy is related to the waves reflected from the plate surface. Moreover, the propagation of elastic waves in the plate is related to the propagation of so-called leaky waves (Fig. 3b). It means that the energy of elastic waves propagating in the plate is transformed back to the acoustic waves propagating in the air. A very important role plays the slope angle θ at which the ACT is oriented in respect to the plate (Fig. 2). The proper assessment of optimal θ angle is thus very important - firstly, to be able to generate desired Lamb wave modes and secondly - to generate them efficiently (large amplitudes of waves). The optimal angle can be calculated based on Snell's law [11]. For this purpose sound wave velocity in the air and phase velocity of desired Lamb wave mode in the specimen with specified material, thickness and excitation frequency needs to be known.

4 Dispersion Curves Extraction

The simplest way to determine the phase velocity of desired wave mode propagating in the GFRP plate is to extract the dispersion curves. For this purpose, elastic waves were excited by the PZT bonded to the structure in the middle of the plate. Excitation signal in the form of five cycles of sine with a carrier frequency of 40 kHz modulated by the Hann window was used. Full wavefield measurements of elastic waves were performed using SLDV. The gathered time-space domain signals in the form of 3D matrix were then transformed to the frequency-wavenumber domain using 3D fast Fourier transform (FFT). Based on the transformed results, dispersion curves were determined and presented in the Fig. 4. This plot in form of the map was created along the direction of reinforcing fibres. Based on the knowledge from previous research related to this sample [12], the authors claimed that the propagation of A0 wave mode can be noticed in Fig. 4. The energy of waves is concentrated in narrow frequency band related to the excitation tone burst signal. Based on it, the wavenumber k was extracted for the frequency of 40 kHz and then the phase velocity of A0 mode was calculated. Next, using the Snell law the optimal ACT slope angle $\theta = 32°$ for A0 mode generation was determined.

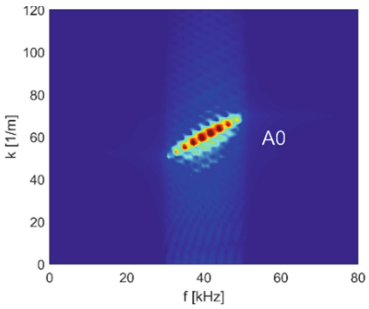

Fig. 4. Dispersion map for elastic waves excitation based on the piezoelectric transducer.

Next, elastic waves were generated using the ACT. Two cases were considered: ACT oriented at the optimal angle $\theta = 32°$ and ACT oriented at the angle $\theta = 0°$ (perpendicularly to the plate). The same procedure in terms of SLDV and dispersion curves extraction process was used. In the Fig. 5a) dispersion map for elastic waves generated by the ACT oriented at the optimal angle $\theta = 32°$ is thus presented. In this case the propagation of A0 mode is similar to the previously considered case (Fig. 4). However, in the case of ACT elastic waves energy is concentrated in narrower frequency band than in the PZT case. It is caused by the fact that ACT is a resonant device working at the frequency of 40 kHz.

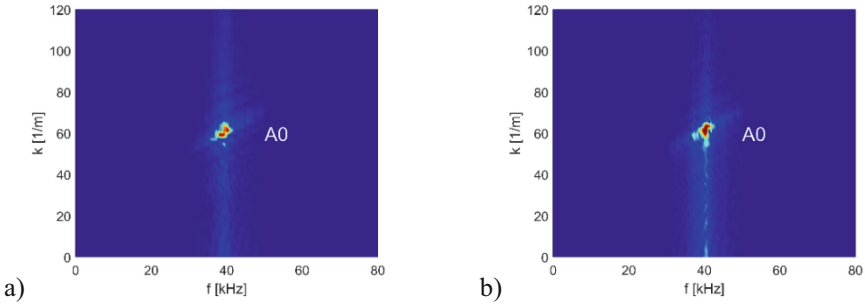

Fig. 5. Dispersion maps for the elastic waves excitation based on ACT at the slope angle: a) $\theta = 32°$, b) $\theta = 0°$.

In the Fig. 5b) dispersion map for elastic waves generation by the ACT oriented at the angle $\theta = 0°$ was presented. Beside of the A0 wave mode, the energy of waves with lower wavenumbers than these corresponding to A0 mode can also be noticed. The wavenumbers related to symmetric S0 wave mode and shear horizontal SH0 mode are located there. However, the generation of pure S0 or SH0 wave mode was not observed.

5 Teflon Inserts Localization Results

As the result of full wavefield measurement in the considered area of the plate, the 3D matrix containing discrete velocity field $v[i, j, k]$ is obtained. The matrix contains the wave signals collected over the whole mesh of measurement points [*i, j*]. Two algorithms of damage imaging were investigated in this research. The first algorithm is based on RMS elastic waves energy values. The second one can be called as the wavefield irregularities mapping (WIM) algorithm [13]. Both algorithms create damage maps (RMS and WIM) which show the damage location and shape. More information about the used algorithms can be found in [13].

5.1 Full Wavefield Results - Piezoelectric Transducer

In the case of a piezoelectric transducer, elastic waves were excited in the middle of the plate. Excitation signal (five cycles of sine, modulated by Hann window) with carrier frequency 40 kHz was utilized. In the Fig. 6a) RMS elastic waves energy map is shown. Elastic waves energy is the highest in the region where the PZT is located. The energy is concentrated in horizontal and vertical direction running through the waves generation point. It is related to the reinforcing fibres orientation in GFRP panel (0/90°). Teflon inserts T1 ÷ T4 (Fig. 1) caused disturbances in the elastic waves energy distribution. However, RMS energy maps do not indicate the clear location and shape of Teflon inserts. In the Fig. 6b) WIM damage map is presented. Similarly as in the RMS case, guided waves energy is concentrated mainly in the location of PZT. Moreover, the waves energy is concentrated in the locations of Teflon inserts T1 ÷ T4. It is caused by the interactions of elastic waves with Teflon inserts (the waves reflections, the waves entrapment) [11]. Locations of all Teflon inserts are indicated but the shape is not determined precisely. In the next step, similar wave energy maps were created for the ACT-based elastic waves generation.

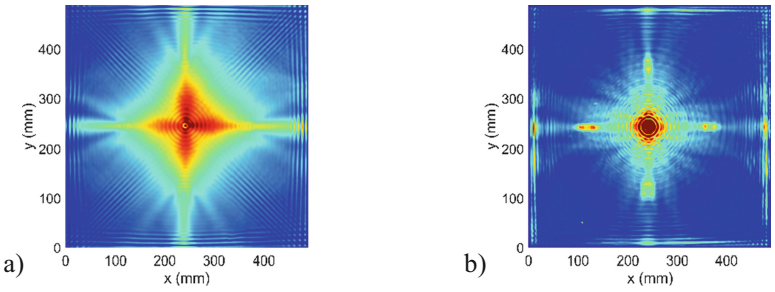

Fig. 6. Damage imaging maps (PZT excitation): a) RMS, b) WIM.

5.2 Full Wavefield Results - Air-Coupled Transducers

In case of the one ACT, two transducer slope angles $\theta = 0°$ and $\theta = 32°$ were investigated. In addition, the case with four ACTs oriented at the angle $\theta = 32°$ (optimal angle for A0 mode generation) was investigated. In this case, four ACTs were generating the waves simultaneously. The investigated ACTs configurations are presented in the Fig. 7.

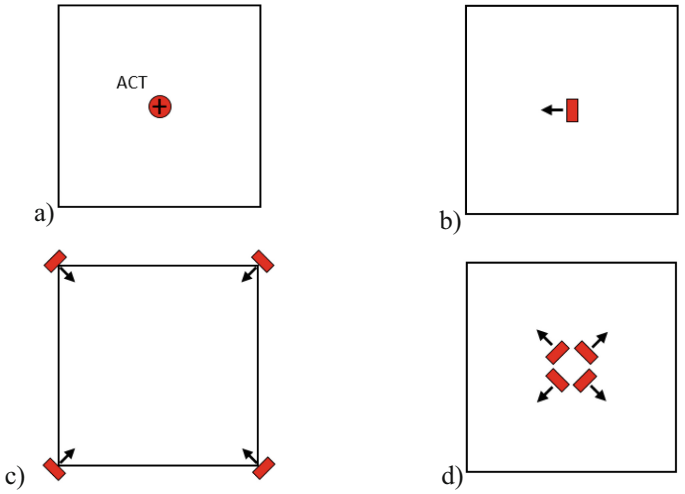

Fig. 7. Different ACTs configurations: a) ACT at θ = 0°, b) ACT at θ = 32°, c) 4× ACTs at θ = 32° in the plate corners, d) 4× ACTs at θ = 32° in the middle of the plate.

In the first case one ACT oriented at the angle θ = 0° was investigated (Fig. 7a). The second case is related to one ACT oriented at the optimal angle θ = 32° (Fig. 7b). In the third case four ACTs adjusted at the plate corners with the optimal angles θ = 32° were investigated (Fig. 7c). In the fourth case, four ACTs located in the middle of the plate area and sloped with the angle θ = 32° were investigated (Fig. 7d).

In the Fig. 8a) RMS elastic waves energy map for the ACT oriented at the angle θ = 0° is presented. This map looks similar to the RMS map based on the PZT usage (Fig. 6a). Elastic waves energy is the highest in the region where the acoustic waves are falling on the specimen (i.e. the middle plate area). Elastic waves energy is also concentrated along directions of the reinforcing fibres. The interactions of elastic waves with Teflon inserts are not so clearly visible like in the case of PZT-based excitation. In the Fig. 9a) the WIM results for the ACT case is presented. In this case the locations of Teflon inserts are clearly visible. However, the shapes of inserts could not be clearly determined. In the Fig. 8b) RMS elastic waves energy map for the case of ACT oriented at the angle θ = 32° is shown. Elastic waves energy is the highest in the middle of the plate and it is concentrated in one direction (direction of the ACT slope). The angle θ = 32° was optimal for the generation of A0 mode and allows to increase the waves energy for about ∼ 40% in relation to the angle θ = 0°. Furthermore, there is the energy distribution disturbance visible at the location of Teflon insert T4 (Fig. 1).

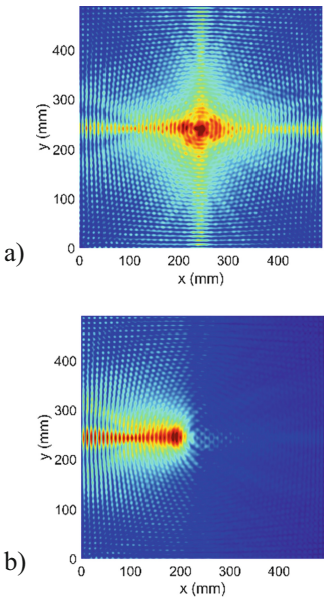

Fig. 8. RMS damage maps for selected ACT slope angles: a) θ = 0°, b) θ = 32°.

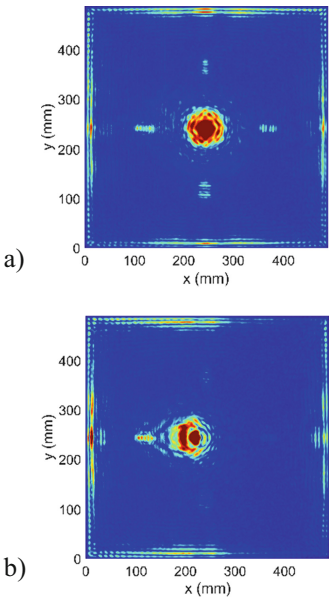

Fig. 9. WIM damage maps for selected ACT slope angles: a) θ = 0°, b) θ = 32°.

In Fig. 9b) the WIM map for the ACT oriented at the angle θ = 0° was presented. In this case the location of Teflon insert T4 is clearly visible. Moreover, the locations of inserts T1 ÷ T3 are also indicated but the energy concentration in their locations is lower than in the case of T4 located in the direction at which the waves energy is focused. Summarizing, using one ACT there is a compromise between the elastic wave energy distribution and the elastic waves amplitude/energy. ACT oriented at the angle θ = 0° generates elastic waves in all directions. However, the amplitude of generated waves (∼A0 mode) is lower than while assuming the optimal angle θ = 32°. In the case of optimal ACT angle, amplitudes of waves are higher but the waves propagation is focused in one direction.

In the case where the damage will be located at the angle of 45°, the waves energy concentration in this direction could be too small to detect this damage. In order to solve this problem, the array of four ACTs was investigated.

In the first case, four ACTs (each one oriented at the angle θ = 32°) located at the plate corners (Fig. 7c) were investigated. ACTs were located in the area outside the plate. RMS waves energy map for this case is presented in the Fig. 10a). In this case, elastic waves energy is concentrated in the corners of the plate where the acoustic waves initially reach the plate and they are converted to elastic waves. There are no energy disturbances related to Teflon inserts locations. Most of the elastic waves energy is concentrated along with the directions of −45°/45°. In the Fig. 11a) WIM damage map is presented for the investigated case. This time the locations of Teflon inserts T2 ÷ T4 are indicated. Elastic waves energy concentration in the locations of inserts is smaller than in the case of one ACT oriented at the angle θ = 0° (Fig. 9a).

Next, the configuration of four ACTs (each one oriented at the angle θ = 32°) located in the middle of the plate area was investigated (Fig. 7d)).

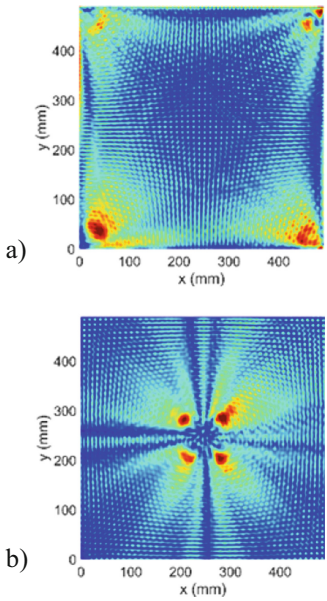

Fig. 10. RMS damage maps for 4 ACT: a) at plate corners, b) in the middle of the plate; slope angle θ = 32°.

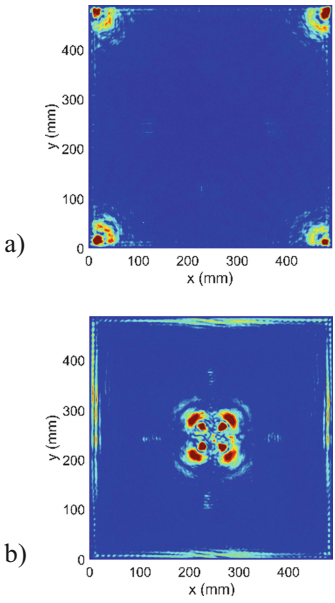

Fig. 11. WIM damage maps for 4 ACT: a) at plate corners, b) in the middle of the plate; slope angle θ = 32°.

In the Fig. 10b) the RMS energy map for this case is presented. Elastic waves energy is concentrated in the four regions in the middle of the plate (the locations where the acoustic waves from ACTs reach the plate surface). Elastic waves energy is concentrated along directions of −45°/45° and also (partially) of 0°/90°. In the Fig. 11b) the WIM damage map is presented for the analyzed case. Now, the locations of four Teflon inserts can be finely noticed. There is smaller level of energy in the area of Teflon inserts than in the case of one ACT at the angle θ = 0° (Fig. 9a)). However, such configuration could be more effective for the case of damages oriented at angles −45°/45° for composite plates with the reinforcing fibres orientation of (0°/90°).

6 Conclusions

In the case of one ACT oriented at the angle θ = 0° and in the case of PZT, the artificial damage localization results are similar. It could be observed within the RMS as well as the WIM damage maps.

Elastic waves energy is concentrated mostly along the directions of reinforcing fibres (0°/90°). Hence, the sensitivity of the damage localization algorithms for the case of damages located out of the directions of reinforcing fibres (e.g. −45°/45°) would be much lower.

In the case of one ACT oriented at the angle $\theta = 32°$ which is the optimal angle for generation of A0 elastic wave mode, the generated waves energy is higher than at the angle $\theta = 0°$ but elastic waves are focused along one direction (not the whole area of the plate is covered with elastic waves with large energy).

In the cases of four ACTs located in the corners of the plate and in its middle, elastic waves energy is concentrated mainly along the directions of −45°/45°. It allows to increase the sensitivity of damage detection if this damage is not located in the direction of reinforcing fibres (0°/90°). Teflon inserts locations were better indicated in the case of four ACTs located in the middle. However, the array of four ACTs located around the corners (transducers mounted outside of the plate area) allows for generation and measurements of elastic waves on one side (i.e. the access from one side of the structure is possible).

In the case of PZT and ACTs, only antisymmetric A0 wave mode was excited for the investigated excitation frequency of 40 kHz. The propagation of SH0 and S0 elastic wave modes was not observed.

The usage of non-contact ACT-based elastic waves generation could be useful in structures where PZTs cannot be used (e.g. the case when it is not allowed to bond anything on a structure surface, the case when high temperatures over Curie point exist).

Acknowledgements. The authors would like to gratefully acknowledge the support given by the National Science Centre, Poland under grant agreement no. 2018/31/B/ST8/01298 in the frame of OPUS project entitled: "Phenomenon of conversion of the acoustic waves to elastic waves due to interactions with solids".

References

1. Wang, B., Zhong, S., Lee, T.L., Fancey, K.: Non-destructive testing and evaluation of composite materials/structures: a state-of-the-art review. Adv. Mech. Eng. **12**(4) (2020)
2. Bustamante, L., Jeyaprakash, N., Yang, C.-H., Tseng, S.-P.: Nondestructive characterization of mechanical properties on metallic and polymer plates using hybrid laser-air coupled ultrasonic techniques. Int. J. Adv. Manuf. Technol. **112**(5–6), 1767–1785 (2021). https://doi.org/10.1007/s00170-020-06463-8
3. Xiao, W., Yu, L.: Nondestructive evaluation with fully non-contact air-coupled transducer-scanning laser Doppler vibrometer Lamb wave system. In: Proceedings of SPIE, Nondestructive Characterization and Monitoring of Advanced Materials, Aerospace, Civil Infrastructure and Transportation, vol. XIII, p. 10971 (2019)
4. Álvarez-Arenas, T.E.G.: Simultaneous determination of the ultrasound velocity and the thickness of solid plates from the analysis of thickness resonances using air-coupled ultrasound. Ultrasonics **50**(2), 104–109 (2010)
5. Li, Y., He, C., Lyu, Y., et al.: Crack detection in monocrystalline silicon solar cells using air-coupled ultrasonic lamb waves. NDT E Int. **102**, 129–136 (2019)
6. Marhenke, T., Neuenschwander, J., Furrer, R.: Modeling of delamination detection utilizing air-coupled ultrasound in wood-based composites. NDT E Int. **99**, 1–12 (2018)

7. Vössing, K.J., Gaal, M., Niederleithinger, E.: Imaging wood defects using air coupled ferroelectret ultrasonic transducers in reflection mode. Constr. Build. Mater. **241**(30), 110832 (2020)
8. Yilmaz, B., Asokkumar, A., Jasiūnienė, E., et al.: Air-coupled, contact, and immersion ultrasonic non-destructive testing: comparison for bonding quality evaluation. Appl. Sci. **10** (19), 6757 (2020)
9. Evani, S.K., Spalvier, A., Popovics, J.S.: Air-coupled ultrasonic assessment of concrete rail ties. NDT E Int. **123**, 102511 (2021)
10. Boccaccio, M., Fierro, G.P.M., Meo, M., et al.: Development and focusing enhancement of nonlinear air-coupled acoustic technique for damage characterization in materials. Mater. Today Proc. **34**(1), 266–274 (2021)
11. Wandowski, T., Mindykowski, D., Kudela, P., Radzienski, M.: Analysis of air-coupled transducer-based elastic waves generation in CFRP plates. Sensors **21**(21), 7134 (2021). https://doi.org/10.3390/s21217134
12. Wandowski, T., Malinowski, P., Kudela, P., Ostachowicz, W.: Analysis of S0/A0 guided wave mode conversion phenomenon. In: Proceedings SPIE 10600, Health Monitoring of Structural and Biological Systems, vol. XII, p. 1060028 (2018)
13. Radzienski, M., Kudela, P., Marzani, A., et al.: Damage identification in various types of composite plates using guided waves excited by a piezoelectric transducer and measured by a laser vibrometer. Sensors **19**, 1958 (2019)